HOKKAIDO UNIVERSITY

Title	Influence of silicon on the growth of barrier-type anodic films on titanium
Author(s)	Tanvir, M. Tauseef; Fushimi, K.; Shimizu, K. et al.
Citation	Electrochimica Acta, 52(24), 6834-6840 https://doi.org/10.1016/j.electacta.2007.04.113
Issue Date	2007-08-01
Doc URL	https://hdl.handle.net/2115/27971
Type	journal article
File Information	ECA52-24.pdf

Hokkaido University Collection of Scholarly and Academic Papers : HUSCAP

Influence of Silicon on the Growth of Barrier-Type Anodic Films on Titanium

M. Tauseef Tanvir*, K. Fushimi*, K. Shimizu**, S. Nagata†, P. Skeldon‡, G.E. Thompson‡ and H. Habazaki*, [a]

*Graduate School of Engineering, Hokkaido University, N13-W8, Sapporo 060-8628, Japan

**University Chemical Laboratory, Keio University, 4-1-1, Hiyoshi, Yokohama 223-8521, Japan

†Institute for Materials Research, Tohoku University, 2-1-1, Katahira, Sendai 980-8577, Japan

‡Corrosion and Protection Centre, School of Materials, The University of Manchester, P.O. Box 88, Manchester M60 1QD, UK

[a]Corresponding author: phone&fax: +81-11-706-6575; e-mail: habazaki@eng.hokudai.ac.jp

Abstract

Amorphous anodic titania, stabilised by incorporation of silicon species, is shown to grow to high voltages on sputter-deposited, single-phase Ti-Si alloys during anodizing at a constant current density in ammonium pentaborate electrolyte. The films comprise two main layers, with silicon species confined to the inner layers. An amorphous-to-crystalline transition occurs at ~60 V on the Ti-6 at% Si alloy, while the transition is suppressed to voltages above 140 V on alloys with 12 and 26 at% silicon. The crystalline oxide, nucleated at a depth of ~40% of the film thickness, is associated with the presence of a precursor of crystalline oxide in the pre-existing air-formed oxide. The modified structure of the air-formed oxide due to increased incorporation of silicon species suppresses the amorphous-to-crystalline transition until the onset of dielectric breakdown. The transport numbers of cations and anions during growth of the anodic oxides are independent of the concentration of silicon species in the inner layer, despite the marked change in the field strength.

Keywords: anodic oxide, ionic transport, anodic titania, amorphous-to-crystalline transition

1. Introduction

Anodic titanium oxide has attracted much attention due to its potential widespread applications, including photocatalysis, photovoltaics, sensors and capacitors [1]. Such interest in the anodic titanium oxide has been enhanced by the recent development of self-organized porous anodic titanium nanotubes in fluoride-containing electrolytes [2, 3]. For capacitor applications in the microelectronics industry, a dense and flaw-free barrier oxide must be formed as a dielectric layer. In contrast to anodic aluminium oxide (ε_{ox} = 10) and tantalum oxide (ε_{ox} = 27), which are currently used in commercial electrolytic capacitors, anodic oxide films develop with a high population density of flaws on high purity titanium in aqueous electrolytes. Thus, anodic titanium oxide-based capacitors have not been realized practically despite the large permittivity of the oxide [4].

The development of flaws in anodic titanium oxide is associated with crystallisation of the anodic oxide during anodizing. Initially, the anodic film is amorphous, but an amorphous-to-crystalline transition occurs at voltages of less than 10 V [4]. The crystalline oxide in the film provides an electron-conducting path, which enables oxygen generation to occur on crystalline regions [5]. From transmission electron microscopy (TEM) of ultramicrotomed sections, the crystalline oxide is formed in the inner part of the films, where the film material is developed at the metal/film interface [6]. The crystalline oxide develops further during thickening of the anodic film, being evident from the increased size of crystalline regions with increasing distance from the metal/film interface. Gas bubbles generated at the crystalline regions in the anodic films are directly observed by TEM, and increased gas pressure in the bubbles with film growth results in the breakdown of the anodic film. The previous findings suggest that crystalline oxide is nucleated when the titanium oxide is developed at the metal/film interface, while the film material in the outer region, formed at the film/electrolyte interface, is only amorphous.

It is well known that crystallisation of amorphous anodic oxides is impeded by incorporation of foreign species. For instance, electron beam-induced crystallisation of anodic alumina during TEM observation is delayed in the outer film regions containing electrolyte-derived species [7]. For anodic titanium oxide, effective suppression of crystallisation has been demonstrated by incorporation of silicon species from the metal substrate, i.e., anodizing of a Ti-6 at% Si alloy [6, 8, 9]. Alloying of titanium with other metals, such as aluminium, molybdenum, niobium, tungsten and zirconium, is also effective, although higher concentrations of alloying elements, compared with silicon addition, are required to form amorphous oxide without crystallisation to voltages higher than 100 V [10].

Even for the Ti-6 at% Si alloy, crystalline oxide is formed at increased voltages, but the crystals are nucleated only at a depth of ~40% of the film thickness [6]. Since the transport number of cations in the growing anodic oxide is approximately 0.4 [8, 9], the depth of the crystals corresponds to the boundary between film material developed by outward migration of cations and inward migration of anions. In general, amorphous anodic oxide grows due to simultaneous migration of outwardly mobile cations and inwardly mobile anions through a pre-existing air-formed oxide. The development of crystalline oxide only at the marker plane suggests that its nucleation is associated with the air-formed oxide; no crystals are nucleated when the oxide is developed at the alloy/film interface. In fact, an influence of ageing of the air-formed oxide on crystallisation of anodic oxide has been reported [6].

In this work, for a further understanding of the amorphous-to-crystalline transition of the anodic oxide, the influence of silicon content in Ti-Si alloys on the growth and crystallization of the anodic oxide has been examined using TEM, Rutherford backscattering spectroscopy (RBS) and X-ray photoelectron spectroscopy (XPS). The dielectric properties of the resultant anodic oxides have also been examined by impedance spectroscopy.

2. Experimental

Ti-Si alloy films, containing 6, 12 and 26 at% silicon, as well as 99.9% pure titanium, were prepared by dc magnetron sputtering on to glass plates and aluminium sheets. The aluminium sheet was electropolished and then anodized to 200 V in 0.1 mol dm^{-3} ammonium pentaborate electrolyte to develop a relatively smooth surface. The target consisted of a 99.9% pure titanium disk of 100 mm diameter and 6 mm thickness; for the preparation of alloy films, one, two and four square silicon plates, with 15 mm sides, were placed symmetrically on the region of the target that is sputtered. In order to generate deposited films of uniform composition and thickness, the substrate holders were rotated around the central axis of the chamber as well as their own axes. The compositions of the deposits were examined by RBS and the structures were determined by X-ray diffraction (XRD) using Cu Kα radiation.

The deposited films were anodized to selected voltages at a constant current density of 50 A m^{-2} in stirred 0.1 mol dm^{-3} ammonium pentaborate electrolyte at 293 K without current decay. A platinum sheet was used as a counter electrode.

Electron transparent sections, ~10 nm thick, of anodized specimens were obtained by a RMC MT-7 ultramicrotome for TEM observation. Briefly, encapsulated specimens were trimmed initially with glass knives, and then suitably thin sections were obtained with a diamond knife. The sections were examined by JEOL JEM 2000FX transmission electron microscope operated at 200 kV. Compositions of the alloy and anodic films were determined by RBS using 2.0 MeV He^{2+} ions. The scattered particles were detected at 170° to the incident beam direction, which was normal to the specimen surface. The data were analysed using RUMP program [11]. XPS spectra of the as-deposited specimens were also measured using SHIMADZU ESCA-3200 spectrometer with Mg Kα excitation (hν = 1253.6 eV). Binding energies of the photoelectrons were calibrated by a method described elsewhere [12].

Dielectric properties of the anodic oxides were examined by an electrochemical

impedance technique. The impedance and the phase shift were measured in 0.1 mol dm^{-3} ammonium pentaborate electrolyte at an open circuit potential with an ac amplitude of 20 mV over a frequency range of 10 mHz to 100 kHz.

3. Results

3.1 XRD patterns

Figure 1 shows the XRD patterns of the as-deposited titanium and Ti-Si alloys. The pattern of the deposited titanium reveals an hcp structure, with a strong 002 line indicating (001) preferred orientation of the deposit. The pattern of the Ti-6 at% Si is similar to that of titanium, but the 002 line shifts slightly to higher angles due to dissolution of silicon in titanium. Further increase in silicon content reduces the diffraction intensity markedly, indicating a less crystalline or amorphous deposit. A halo pattern observed around 20-30º originates from the glass substrate. Since the equilibrium solubility of silicon in hcp titanium is less than 1 at% [13], the deposited alloys are non-equilibrium, single-phase solid solutions supersaturated with silicon.

3.2 Voltage-time response

Voltage-time responses of the titanium and Ti-Si alloys (Fig. 2) reveal an initial voltage surge of about 2 V at the commencement of anodizing, reflecting the presence of an air-formed film. Subsequently, the formation voltage increases linearly with time. The linear voltage rise continues to voltages less than 20 V for titanium; thereafter the formation voltage rises at progressively increased rates, followed by a markedly reduced rate of ~1.5 V s^{-1} above 30 V. Evolution of oxygen gas was visible to the naked eye above 30 V. The forming voltage for the Ti-6 at% Si alloy rises linearly to ~60 V, with the slope increasing at higher voltages until film breakdown occurs at about 95 V. The change in the slope at lower formation voltage

compared with that previously reported for the present Ti-6 at% Si alloy [9] is associated with ageing of the deposited films in laboratory air for more than one month [6]. Ageing induces the development of precursor of crystalline oxide in the air-formed oxide, resulting in the nucleation of crystalline oxide at reduced formation voltages during anodizing. For the Ti-12 at% Si and Ti-26 at% Si alloys, the linear rise of formation voltage continues to the breakdown voltages, which are above 140 V. The slope in the linear growth region increases with the silicon content, from 1.39 V s^{-1} for the Ti-6 at% Si alloy to 1.90 V s^{-1} for the Ti-26 at% Si alloy.

3.3 TEM observations

Transmission electron micrographs of ultramicrotomed sections for the three alloys after anodizing to selected voltages are shown in Figs. 3(a)-(c). The selected area electron diffraction patterns of the respective alloy films are also revealed in the micrographs. The electron diffraction of the Ti-6 at% Si alloy discloses an hcp structure, while those of the alloys containing 12 and 26 at% silicon reveal a diffuse ring, typical of amorphous material. These electron diffraction patterns are consistent with the XRD patterns of Fig. 1.

The anodic film formed on the Ti-6 at% Si alloy to 75 V, where the rise of formation voltage is no longer linear with anodizing time, is mainly amorphous; however, crystalline regions are evident at a depth of ~40% of the film thickness. At the region indicated by the arrow, relatively large areas of crystalline oxide are developed with gas bubbles generated around them. As a consequence, the anodic film is slightly thinner than in the surrounding regions. In contrast, the anodic films formed on the alloys with higher silicon contents are totally amorphous, even to a formation voltage of 100 V. The thicknesses of the anodic films are 194 and 150 nm for the Ti-6 at% Si and Ti-26 at% Si alloys respectively. The films appear to comprise two layers; an inner layer, 68% of the film thickness, has a light appearance for

both the alloys. A further increase in contrast difference between the layers is observed for the Ti-26 at% Si alloy. The light appearance of the inner layer is associated with the presence of silicon species only in the inner layer, as shown by later RBS analyses.

3.4 Rutherford backscattering spectroscopy

Figure 4 shows experimental and simulated RBS spectra for the alloy specimens anodized to selected voltages. Simulated spectra, obtained using compositions, thicknesses and densities in Table 1, show good fit to the respective experimental spectra. It is known that boron species are incorporated into the outer part of the anodic film, to a depth of approximately 20% of the film thickness, on the Ti-Si alloys [9]. In the present RBS analyses of the anodic films, however, the presence of boron species is neglected due to difficulty of detection of such a light element at low concentration. In the spectrum of the anodized Ti-6 at% Si alloy, the titanium yield shows a step due to the formation of an anodic film composed mainly of TiO_2. A slight depression of the titanium yield before the edge of the alloy/film interface is associated with the presence of silicon species. The depression is more significant for the alloys with increased silicon contents. From comparison of the compositions of the inner layer of the anodic film and the alloy film, shown in Table 1, it is evident that silicon enriches in the inner layer of the anodic film. The charges required to form the anodic films, calculated from the numbers of tetravalent titanium and silicon cations, were similar to those passed during anodizing to selected formation voltages to an accuracy of 5%, indicating that the efficiency of film formation during anodizing is close to 100%.

3.5 XPS analyses

XPS spectra of the as-deposited alloy specimens were measured to examine the composition of the air-formed films present before anodizing. Ti 2p spectra of the

as-deposited specimens, shown in Fig. 5(a), reveals a major peak at 459.1 eV, corresponding to Ti^{4+} species, with a small peak at 453.7 eV for metallic titanium. The Si 2p spectra, shown in Fig. 5(b), disclose the presence of oxidised silicon species, which appears at 102.3 eV. This binding energy corresponds to the tetravalent silicon species. Metallic silicon species appear at 98.5 eV. Thus, the air-formed films formed on the Ti-Si alloys contain silicon species, and from the increased intensity of oxidised silicon species with increased silicon content in the alloy, the concentration of silicon species in the air-formed oxide is increased.

3.6 Dielectric properties

Since uniform anodic films were grown to relatively high voltages for all the Ti-Si alloys examined, dielectric properties of anodic films were examined by ac impedance spectroscopy. Figure 6 shows Bode plots of the alloy specimens anodized to 50 V. All the alloys revealed a linear voltage to the selected voltage (Fig. 2). The Bode plots indicate dominance of the capacitance of the anodic film in the frequency range from 0.1 Hz to 1 kHz; the impedance changes approximately linearly with frequency, with a slope of -1 and phase shift close to -90°. Over this frequency range, the impedance increases slightly with increase in silicon content in the alloy, suggesting a reduced capacitance of the anodic film with increased silicon content. At high frequency, above 10 kHz, the impedance is nearly constant at $\sim 70\ \Omega\ cm^2$, which corresponds to the resistance of electrolyte.

The decrease of the capacitance of the anodic film formed at 50 V with the silicon content of the alloy is clearly shown in Fig. 7. Similar to the capacitance, the permittivity of the anodic film decreases with the silicon content. The reduction of the capacitance is less significant than that of permittivity, due to reduced thickness of the anodic film with increased silicon content. Such compositional dependence can be understood from the observation that the permittivities and growth parameters, including field strength and transport numbers of

cations and anions, of the anodic films formed on the binary alloys are compositional averages of those of films on the respective metals [10, 14, 15].

4. Discussion

4.1 Crystallisation of anodic oxide

The present study clearly demonstrates that the amorphous-to-crystalline transition of anodic titanium oxide is hindered by the incorporation of silicon species from substrate. The transition voltage increases with an increase in the silicon content, up to 12 at% Si. For the alloys containing 12 and 26 at% silicon, a linear voltage rise continues to dielectric breakdown at ~140 V (Fig. 2), such that growth of amorphous oxide proceeds until dielectric breakdown. The change in the slope for the Ti-6 at% Si alloy above ~60 V is associated with the development of crystalline oxide as well as gas generation at the crystalline regions (Fig. 3(a)). The increased ionic resistivity of the crystalline oxide, compared with that of respective amorphous oxide, and generated gas bubbles, which also impede the ionic transport in the anodic oxide under the high electric field, contribute to the increased slope. Indeed, thinner oxide layer is developed where large regions of crystalline oxide and gas bubbles are formed (Fig. 3(a)).

The crystalline oxide developed in the anodic film on the Ti-6 at% Si alloy is located only at a depth of ~ 40% of the film thickness; at a region of increased depth, the oxide is amorphous. Thus, the crystallisation is different from that of anodic oxide on high purity titanium, where the crystalline oxide is nucleated immediately above the metal/film interface. The amorphous anodic oxides formed on various valve metals, including titanium, grow simultaneously by cation egress and anion ingress through a pre-existing air-formed oxide. From the transport numbers of cations in growing anodic films on the Ti-Si alloys, the crystalline oxide appears to be developed at the location of the pre-existing oxide. Thus, it is

probable that the pre-existing oxide acts as a nucleation site for crystalline oxide. This is supported by previous work, where ageing of a sputter-deposited Ti-6 at% Si alloy in laboratory air for a prolonged period reduced the voltage for the amorphous-to-crystalline transition [6]. During ageing, a precursor of crystalline oxide is developed. From the XPS spectra shown in Fig. 5, it is clear that silicon species are incorporated into the air-formed oxide, with the concentration increasing with silicon content of the alloy. Silicon species in the air-formed oxide modify the structure of the air-formed oxide, suppressing the development of the precursor of the crystalline oxide, particularly when the concentration is sufficiently high. Thus, anodic films free from crystalline oxides are formed on the Ti-12 at% Si and Ti-26 at% Si alloys.

4.2 Transport numbers of cations and anions

In growing anodic films with an amorphous structure on a range of valve metals, including aluminium[16], niobium[17], tantalum [18-20] and titanium[8, 9], silicon species are known to be immobile. Thus, transport numbers of cations and anions during film growth can be determined from the distribution of silicon species, which act as marker species. In the present anodic films, an outer layer, essentially free from silicon species, is developed at the film/electrolyte interface by egress of titanium ions, while an inner layer containing silicon species is developed at the alloy/film interface by ingress of O^{2-}/OH^{-} ions. The transport number of cations, t_+, can be estimated from the following equation,

$$t_+ = \frac{(N_{Ti})_{out}}{(N_{Ti} + N_{Si})_{film}}$$

in which N_{Ti} and N_{Si} are the numbers of respective ions in the outer layer or total anodic film. These values are shwon from RBS analyses. The transport numbers of cations, calculated from this equation, are plotted in Fig. 8 as a function of the composition of the inner layer. In

the Figure, the apparent field strengths of the inner silicon-containing layer, estimated by assuming a field strength in the outer anodic titanium oxide layer of 0.45 V m^{-1} [4], are also plotted. Despite the marked change in the field strength with the composition of inner layer, the transport number of cations is nearly constant, being 0.42. The value is consistent with previous reports [8, 9, 21].

The transport numbers of cations in growing anodic niobium oxide and tantalum oxide are dependent upon current density and temperature of the electrolyte; for anodic tantalum oxide, the value of t^+ increases with increasing current density and decreases with increasing temperature [22]. A similar trend has been reported for anodic niobium oxide [23]. The findings for anodic niobium and tantalum oxides disclose that the transport numbers of cations are influenced by the field strength in the growing anodic oxides, since the current density and temperature of the electrolyte changes the field strength. Interestingly, the present study demonstrates that the change in field strength due to different concentration of incorporated silicon species does not influence the transport number of cations. The different dependence of the transport number of cations on field strength for the present anodic titanium-based oxide and the niobium and tantalum oxides is not yet understood. Further studies are in progress, which examine the influence of current density and temperature on the transport number of cations in thickening anodic oxides on Ti-Si alloys.

5. Conclusions

1. An amorphous-to-crystalline transition of anodic titanium oxide is impeded by the incorporation of silicon species from substrate. No transition is evident during anodizing of Ti-Si alloys containing 12 at% or more silicon before the dielectric breakdown voltage at ~140 V.
2. The crystalline oxide, developed in the anodic film on the Ti-6 at% Si alloy, is located at

the depth of ~40% of the film thickness. The air-formed oxide present before anodizing acts as a precursor of crystalline oxide.

3. The air-formed oxides on the Ti-Si alloys contain silicon species, with the silicon concentration increasing with the alloy silicon content. The suppression of crystallisation is associated with the modification of the air-formed oxide.
4. The transport number of cations for growing anodic films on the Ti-Si alloys is 0.42, being independent of silicon content, despite the significant change in the field strength.

Acknowledgments

The present work was supported in part by a Grant-in-Aid for Scientific Research, No. 16360353 from the Japan Society for the Promotion of Science.

References

[1] G.K. Mor, O.K. Varghese, M. Paulose, K. Shankar, C.A. Grimes, Sol. Energy Mater., 90 (2006) 2011.

[2] D. Gong, C.A. Grimes, O.K. Varghese, W.C. Hu, R.S. Singh, Z. Chen, E.C. Dickey, J. Mater. Res., 16 (2001) 3331.

[3] V. Zwilling, M. Aucouturier, E. Darque-Ceretti, Electrochim. Acta, 45 (1999) 921.

[4] A. Aladjem, J. Mater. Sci., 8 (1973) 688.

[5] C.K. Dyer, J.S.L. Leach, J. Electrochem. Soc., 125 (1978) 1032.

[6] H. Habazaki, M. Uozumi, H. Konno, K. Shimizu, P. Skeldon, G.E. Thompson, Corros. Sci., 45 (2003) 2063.

[7] K. Shimizu, G.E. Thompson, G.C. Wood, Thin Solid Films, 77 (1981) 313.

[8] H. Habazaki, K. Shimizu, S. Nagata, P. Skeldon, G.E. Thompson, G.C. Wood, Corros. Sci., 44 (2002) 1047.

[9] H. Habazaki, K. Shimizu, S. Nagata, P. Skeldon, G.E. Thompson, G.C. Wood, J. Electrochem. Soc., 149 (2002) B70.

[10] H. Habazaki, H. Konno, K. Shimizu, J. Surf. Finish. Soc. Jpn., 54 (2003) 456.

[11] L.R. Doolittle, Nucl. Instr. and Meth., B9 (1985) 344.

[12] K. Asami, J. Electron Spectrosc. Relat. Phenom., 9 (1976) 469.

[13] T.B. Massalski, *Binary Alloy Phase Diagrams* ed. H. Okamoto. 1990: ASM International.

[14] H. Habazaki, K. Shimizu, P. Skeldon, G.E. Thompson, G.C. Wood, Thin Solid Films, 300 (1997) 131.

[15] H. Habazaki, K. Shimizu, P. Skeldon, G.E. Thompson, G.C. Wood, Proc. R. Soc. Lond. A, 453 (1997) 1593.

[16] G.C. Wood, P. Skeldon, G.E. Thompson, K. Skeldon, J. Electrochem.Soc., 143 (1996) 74.

[17] H. Habazaki, T. Matsuo, H. Konno, K. Shimizu, S. Nagata, K. Matsumoto, K. Takayama, Y. Oda, P. Skeldon, G.E. Thompson, Electrochim. Acta, 48 (2003) 3519.

[18] R.L. Ruth, N. Schwartz, J. Electrochem. Soc., 123 (1976) 1860.

[19] P.J. Silverman, N. Schwartz, J. Electrochem. Soc., 121 (1974) 550.

[20] K. Shimizu, K. Kobayashi, G.E. Thompson, P. Skeldon, G.C. Wood, Philos. Mag. B, 73 (1996) 461.

[21] N. Khalil, J.S.L. Leach, Electrochem. Acta, 31 (1986) 1279.

[22] Q. Lu, P. Skeldon, G.E. Thompson, D. Masheder, H. Habazaki, K. Shimizu, Corros. Sci., 46 (2004) 2817.

[23] S. Ono, M. Baba, M. Shimoyama, H. Asoh, in *Surface Oxide Films*, 2004, Orlando: The Electrochemical Society.

Figure captions

Fig. 1 X-ray diffraction patterns of the sputter-deposited Ti and Ti-Si alloys containing 6, 12 and 26 at% silicon.

Fig. 2 Voltage-time responses of the sputter-deposited Ti and Ti-Si alloys during anodizing at 50 A m^{-2} in 0.1 mol dm^{-3} ammonium pentaborate electrolyte at 293 K.

Fig. 3 Transmission electron micrographs of ultramicrotomed sections for the sputter-deposited (a) Ti-6 at% Si, (b) Ti-12 at% Si and (c) Ti-26 at% Si alloys anodized at 50 A m^{-2} in 0.1 mol dm^{-3} ammonium pentaborate electrolyte at 293 K. The formation voltages are 75 V for Ti-6 at% Si alloy and 100 V for the Ti-12 at% Si and Ti-26 at% Si alloys. The selected area electron diffraction patterns of the respective alloys are also shown

Fig. 4 Experimental and simulated RBS spectra of the sputter-deposited (a) Ti-6 at% Si, (b) Ti-12 at% Si and (c) Ti-26 at% Si alloys anodized at 50 A m^{-2} in 0.1 mol dm^{-3} ammonium pentaborate electrolyte at 293 K. The formation voltages are 75 V for the Ti-6 at% Si alloy and 100 V for the Ti-12 at% Si and Ti-26 at% Si alloys.

Fig. 5 (a) Ti 2p3/2 and (b) Si 2p XPS spectra of the sputter-deposited Ti-Si alloys containing 6, 12 and 26 at% silicon.

Fig. 6 Bode plots, measured in 0.1 mol dm^{-3} ammonium pentaborate, of the anodic films formed to 50 V on the sputter-deposited Ti-Si alloys containing 6, 12 and 26 at% silicon in the same electrolyte at 293 K.

Fig. 7 Changes in capacitance and permittivity of the anodic films formed to 50 V on the sputter-deposited Ti-Si alloys in 0.1 mol dm^{-3} ammonium pentaborate at 293 K as a function of the silicon content in alloy.

Fig. 8 Changes in the apparent field strength and the transport number of cations for the

anodic films formed to 50 V on the sputter-deposited Ti-Si alloys in 0.1 mol dm^{-3} ammonium pentaborate at 293 K as a function of the composition of the inner anodic films.

Table 1 Results of RBS analyses of the sputter-deposited Ti-Si alloys anodized to selected formation voltages at 50 A m^{-2} in 0.1 mol dm^{-3} ammonium pentaborate electrolyte at 293 K.

Alloy	Formation voltage (V)	Thickness (nm)	Composition	Density (Mg m^{-3})
Ti-6 at% Si	75	65	TiO_2	3.8
		85	$(Ti_{0.9}Si_{0.1})O_2$	3.7
Ti-12 at% Si	100	82	TiO_2	3.8
		112	$(Ti_{0.8}Si_{0.2})O_2$	3.6
Ti-26 at% Si	100	65	TiO_2	3.8
		85	$(Ti_{0.55}Si_{0.45})O_2$	3.3

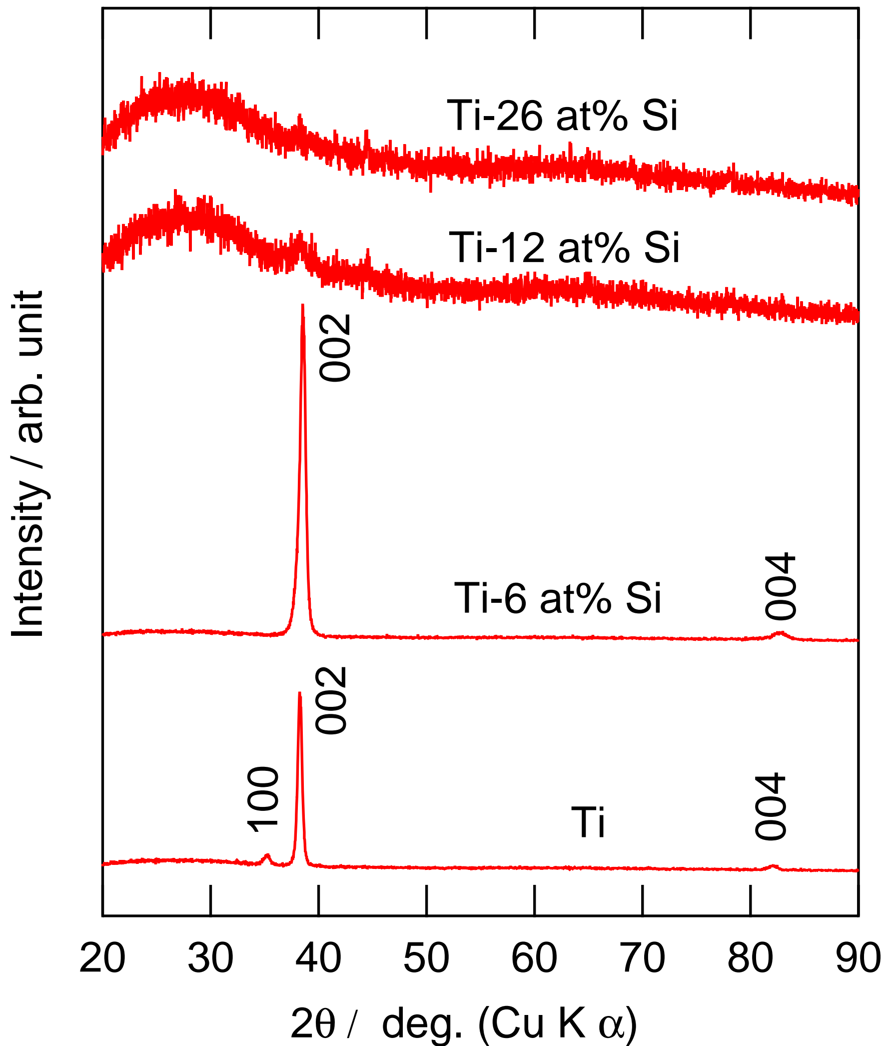
Ti-26 at% Si
Ti-12 at% Si
002
Ti-6 at% Si
004
002
100
Ti
004
Intensity / arb. unit
20
30
40
50
60
70
80
90
2θ / deg. (Cu K α)

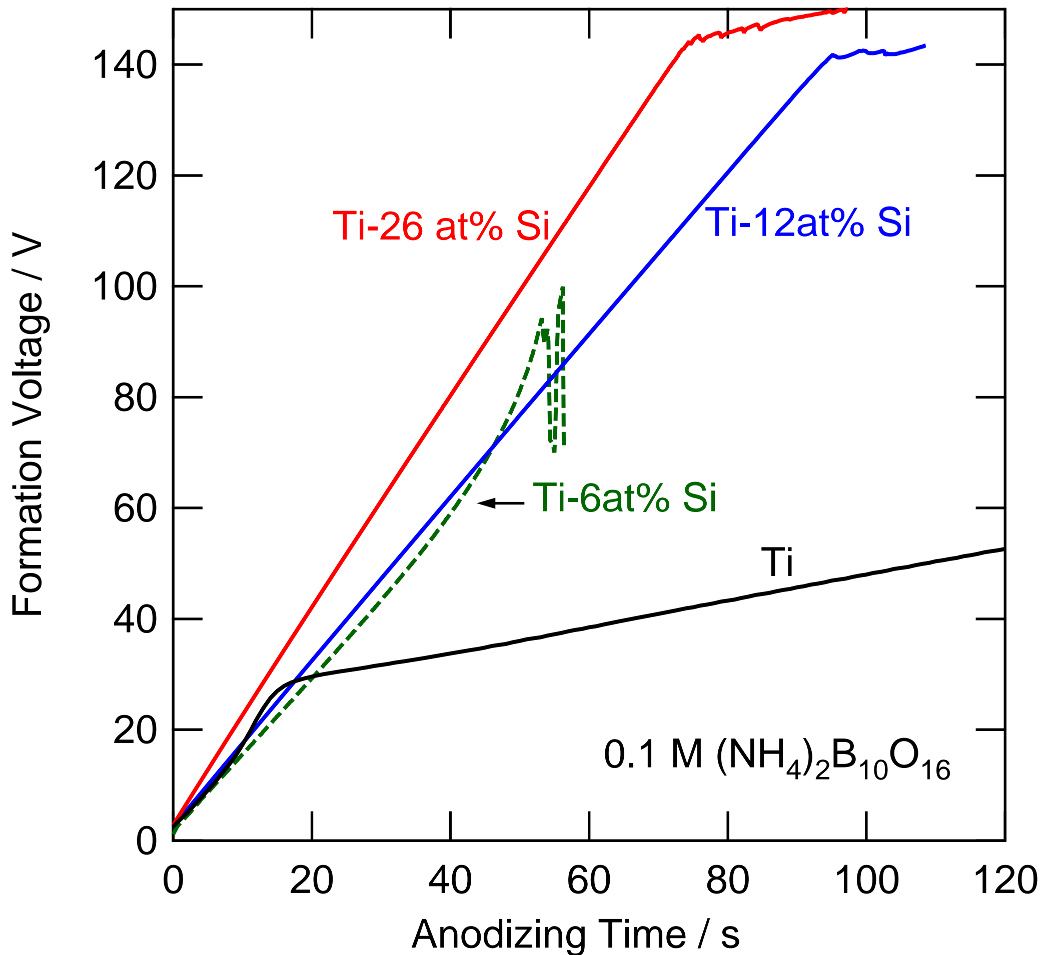

Formation Voltage / V
Anodizing Time / s
Ti-26 at% Si
Ti-12at% Si
Ti-6at% Si
Ti
0.1 M $(NH_4)_2B_{10}O_{16}$
0
20
40
60
80
100
120
140
0
20
40
60
80
100
120

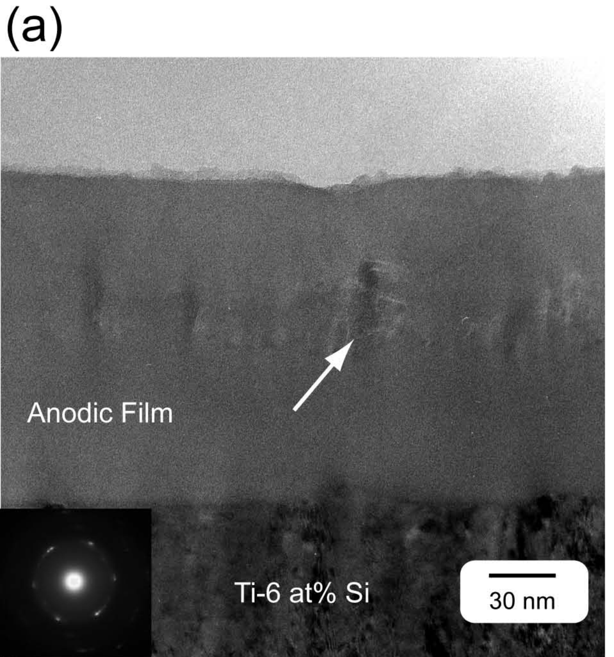
(a)
Anodic Film
Ti-6 at% Si
30 nm

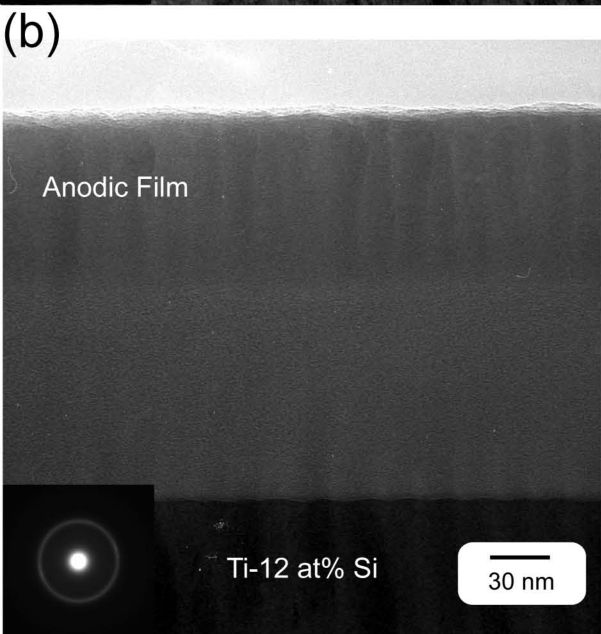
(b)
Anodic Film
Ti-12 at% Si
30 nm

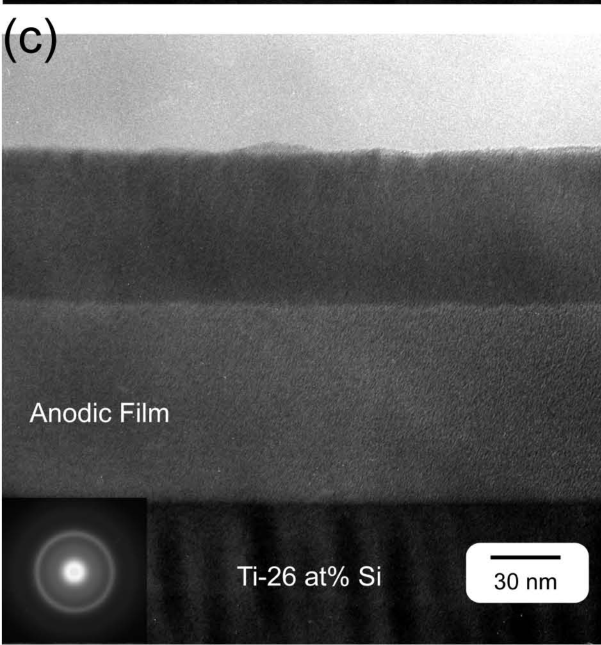
(c)
Anodic Film
Ti-26 at% Si
30 nm

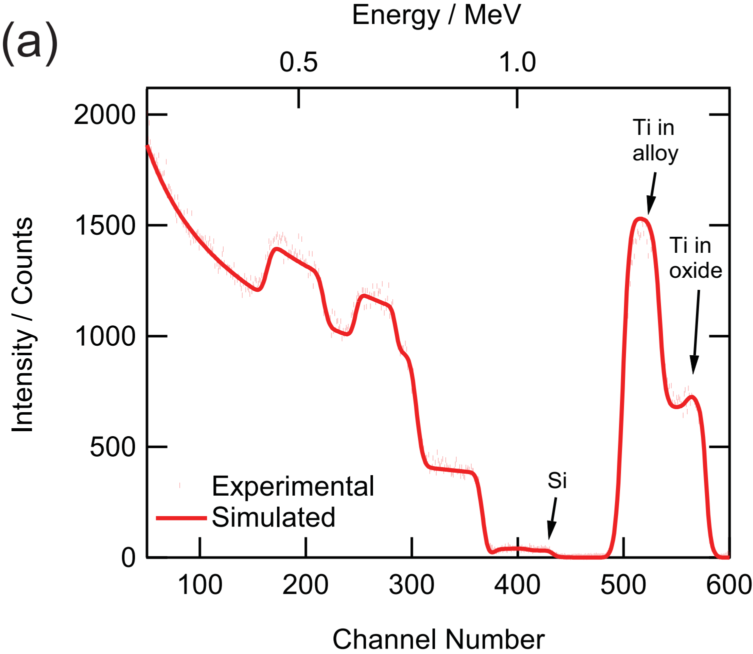
(a)
Energy / MeV
0.5
1.0
2000
1500
1000
500
0
Intensity / Counts
Ti in alloy
Ti in oxide
Si
Experimental
Simulated
100
200
300
400
500
600
Channel Number

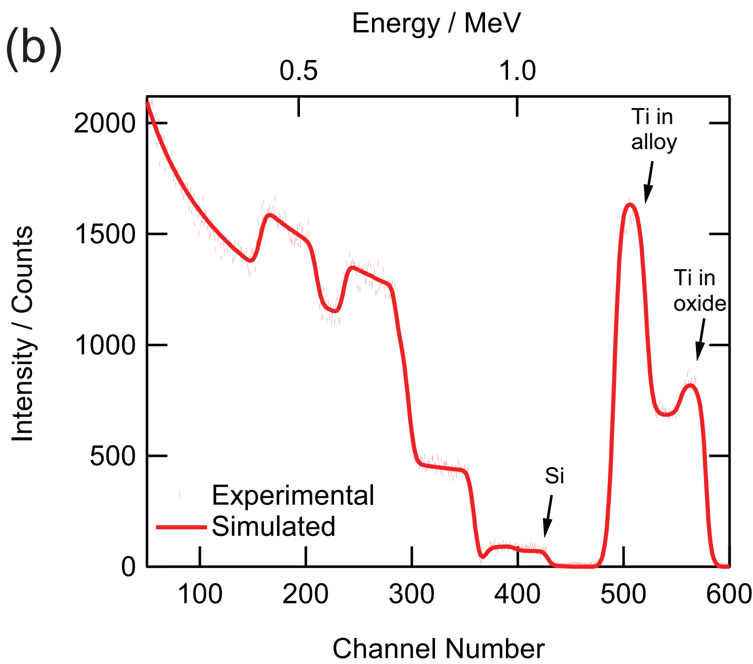
(b)
Energy / MeV
0.5
1.0
2000
1500
1000
500
0
Intensity / Counts
Ti in alloy
Ti in oxide
Si
Experimental
Simulated
100
200
300
400
500
600
Channel Number

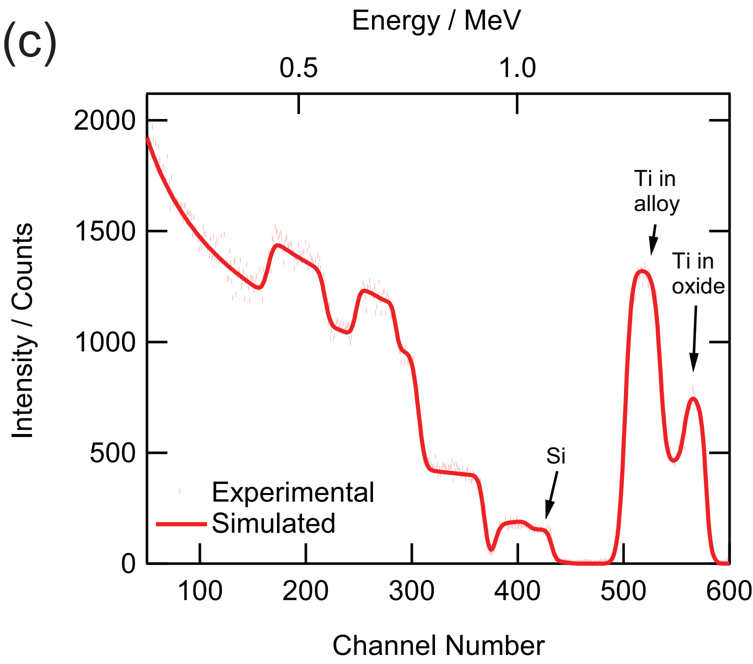
(c)
Energy / MeV
0.5
1.0
2000
1500
1000
500
0
Intensity / Counts
Ti in alloy
Ti in oxide
Si
Experimental
Simulated
100
200
300
400
500
600
Channel Number

(a)

Ti^{4+}

Ti $2p_{3/2}$

Ti^{m}

26 at% Si

12 at% Si

6 at% Si

Intensity / arb. unit

460 456 452 448

Binding Energy / eV

(b)

Si^{4+}

Si 2p

Si^{m}

26 at% Si

12 at% Si

6 at% Si

Intensity / arb. unit

108 104 100 96 92

Binding Energy / eV

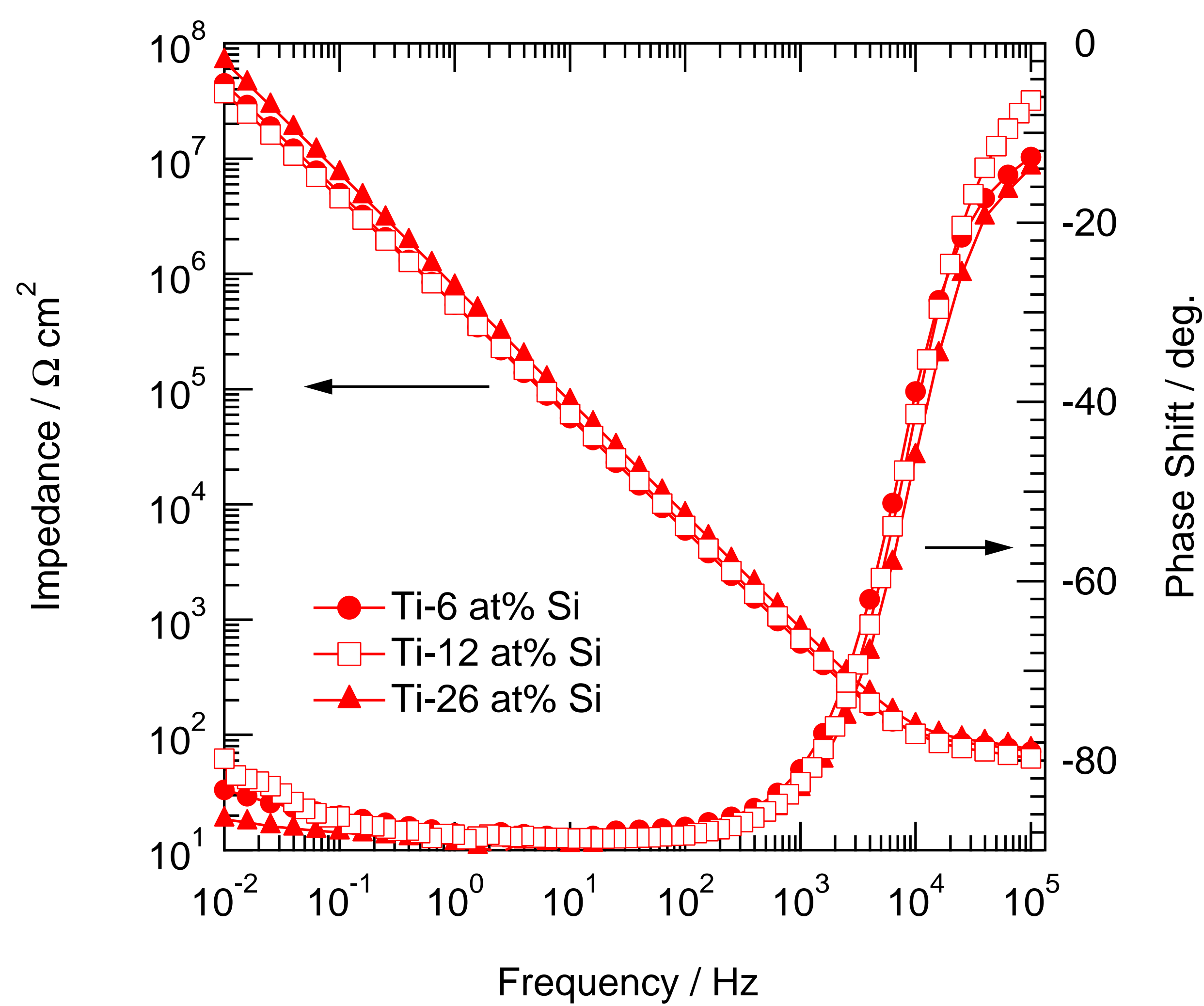

Impedance / Ω cm2
Phase Shift / deg.
Frequency / Hz
Ti-6 at% Si
Ti-12 at% Si
Ti-26 at% Si
10-2
10-1
100
101
102
103
104
105
108
107
106
105
104
103
102
101
0
-20
-40
-60
-80

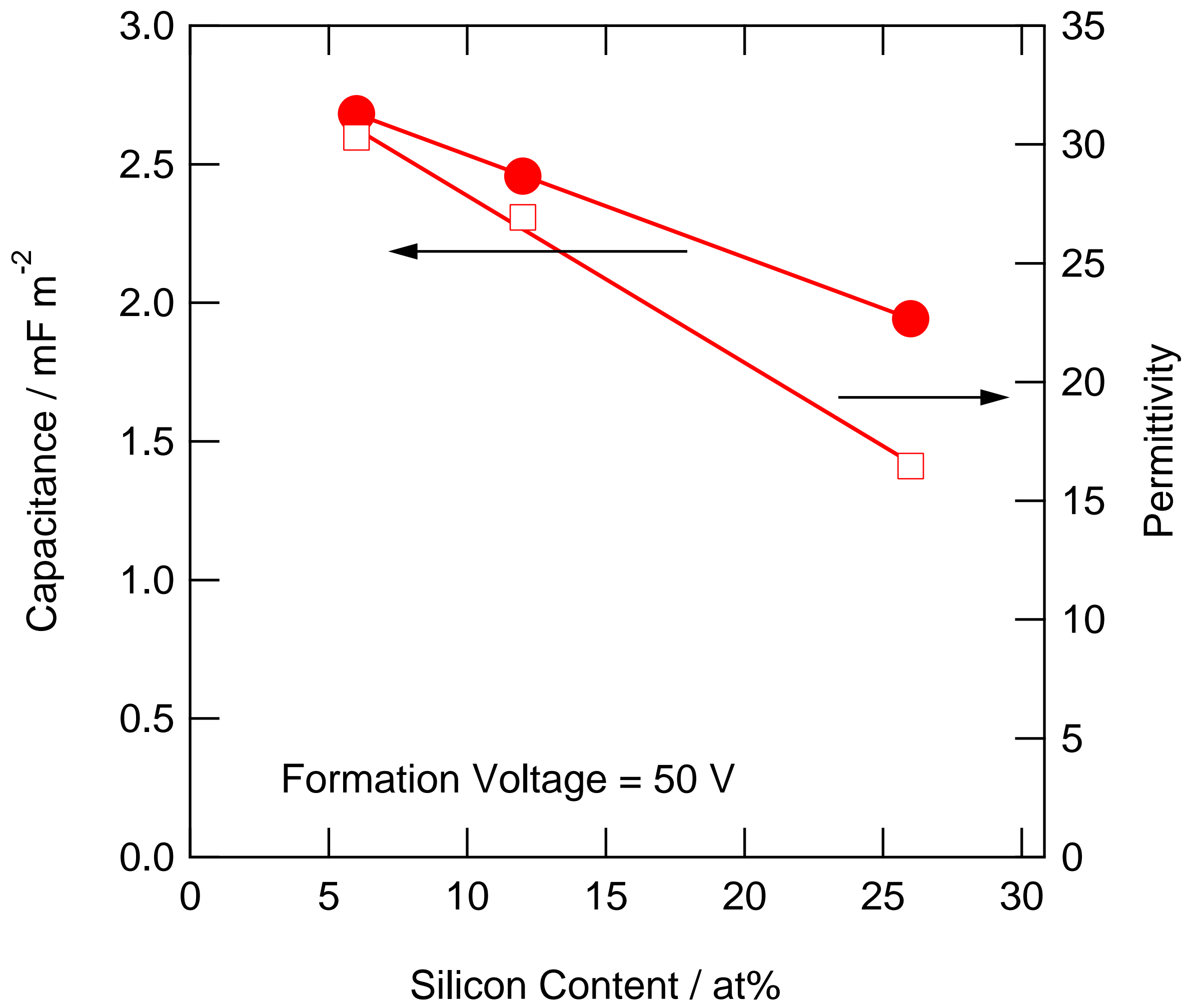

Capacitance / mF m-2
Permittivity
Silicon Content / at%
Formation Voltage = 50 V
3.0
2.5
2.0
1.5
1.0
0.5
0.0
35
30
25
20
15
10
5
0
0
5
10
15
20
25
30

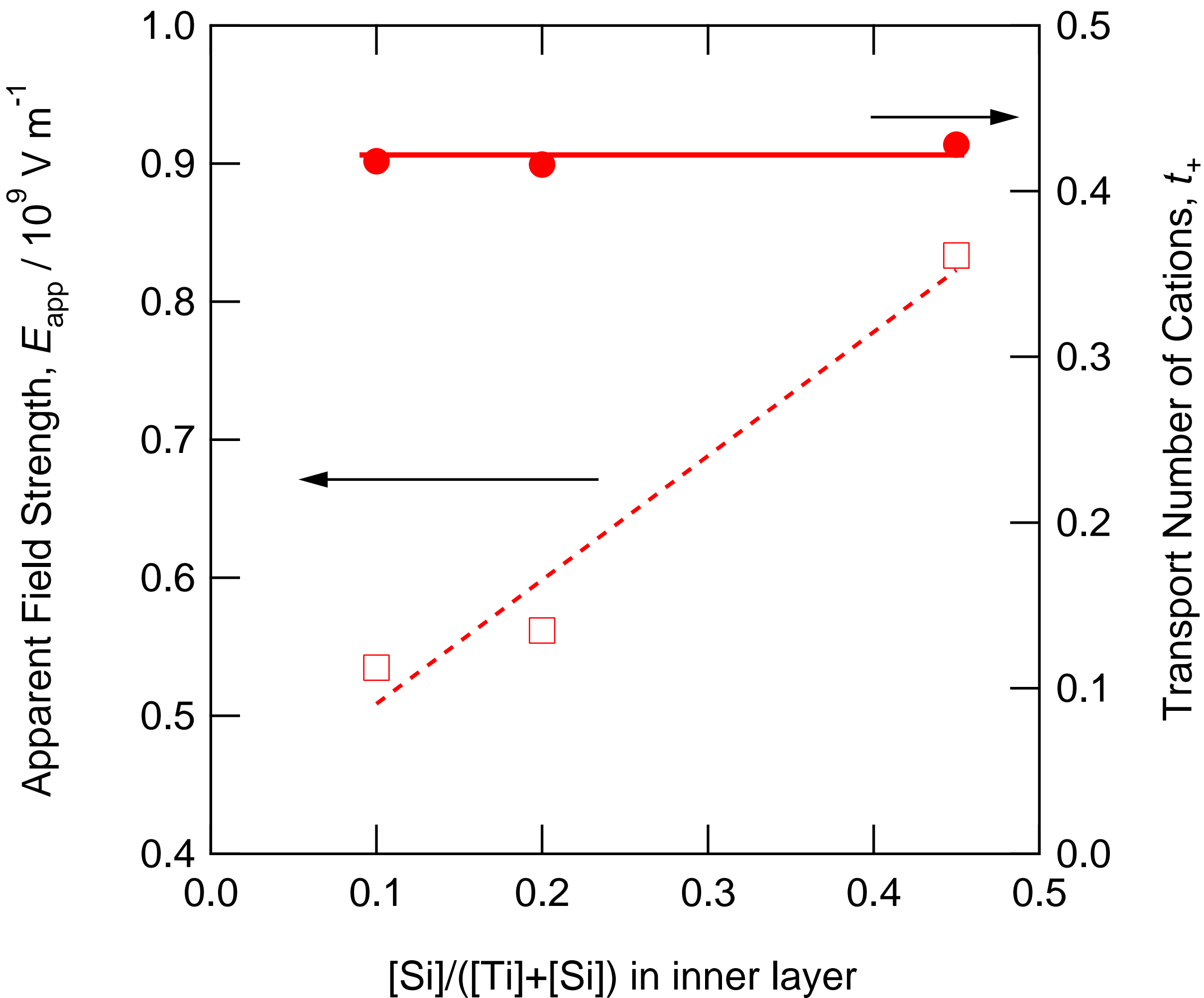

Apparent Field Strength, E_{app} / 10^9 V m^{-1}
Transport Number of Cations, t_+
[Si]/([Ti]+[Si]) in inner layer
1.0
0.9
0.8
0.7
0.6
0.5
0.4
0.0
0.1
0.2
0.3
0.4
0.5